applied optics

Analysis and quantification of collagen organization with the structure tensor in second harmonic microscopy images of ocular tissues

Francisco J. Ávila and Juan M. Bueno*

Laboratorio de Óptica, Instituto Universitario de Investigación en Óptica y Nanofísica Universidad de Murcia, Campus de Espinardo (Ed. 34), 30100 Murcia, Spain
**Corresponding author: bueno@um.es*

Received 8 September 2015; revised 26 October 2015; accepted 28 October 2015; posted 28 October 2015 (Doc. ID 249665); published 16 November 2015

The important biological role of collagen-based tissues and the changes produced in the fiber distribution under particular situations (surgery, pathology, external damage, etc.) require tools for the analysis of the collagen organization that might potentially help in early diagnoses. Since collagen structures provide efficient second harmonic generation (SHG) signals, SHG microscopy has emerged as a powerful technique to visualize collagen fibers and qualitatively discriminate normal from abnormal tissues. Here we propose a quantitative method based on the structure tensor to quantify the different organization of collagen patterns in SHG images of ocular tissues. Results show that well-organized collagen distributions present a high degree of isotropy (DoI), a dominant orientation (PO), and a low structural dispersion (SD). On the other hand, the PO vanishes when the collagen tissue is not organized as a consequence of an increase in the SD and a decrease in the DoI. The proposed method is also able to discriminate partially organized samples. The combination of SHG microscopy and the structure tensor is a useful method to objectively classify collagen distributions. Clinical applications of this technique could help in the diagnosis and tracking of pathologies related to collagen disorders in connective tissue.

OCIS codes: (170.3880) Medical and biological imaging; (180.4315) Nonlinear microscopy; (110.2960) Image analysis; (170.4470) Ophthalmology.

http://dx.doi.org/10.1364/AO.54.009848

1. INTRODUCTION

Connective tissue is mainly composed of collagen fibers, and over 35% of the human body tissues are composed of collagen [1]. Within collagen-based structures, there are more than 20 classified types, of which 80% correspond to type-I collagen [2]. The role of this type of collagen fibers is mainly mechanical, providing strength and stiffness [3], although they are also involved in immunological and metabolic processes [4]. The different types of connective tissues are characterized by the spatial arrangement of the collagen [5]. Since this fiber structural organization is often complex, simplified architecture models have been considered in order to classify collagen structures [6–8].

Second harmonic generation (SHG) is a nonlinear microscopy technique well suited to imaging collagen-based specimens [9], in particular ocular tissues such as the cornea and sclera [10–14]. Collagen distribution can be affected by pathologies, surgery, or thermal procedures, and SHG microscopy has been proven to be a useful tool to visualize those changes [15–17].

The modeling of the structural organization of collagen is a suitable technique to understand early stages of collagen-related pathologies, such as osteogenesis imperfecta [18], cancer [19], or keratoconus [20], among others. Due to this, tools to objectively quantify collagen organization from SHG are often required. There has been an increasing interest in this topic, probably due to its potential clinical applications. The most popular method is based on fast Fourier transform (FFT) algorithms, usually combining analytical and manual procedures [21,22]. Since the parameters associated with the FTT method often fail when the collagen distributions are highly wavy or present cross-hatched patterns, improved procedures have recently been reported [23,24].

In this context the structure tensor is a powerful tool to study and characterize structures and the estimates of patterns of dominant orientations [25–28]. The structure tensor is a matrix of partial derivatives along the x and y directions, containing information about the orientation of every pixel within an image. Although it was introduced for edge detection in

1987 [29], it has also been used for the analysis of biological distributions and modeling of collagen-based tissues [30,31].

In this sense, the aim of this work has been to use the structure tensor to analyze the collagen organization of ocular tissues imaged with SHG microscopy. The implementation of this technique into SHG images will provide a quantitative method to classify the collagen arrangement according to its spatial distribution.

2. METHODS

A. Structure Tensor

Let us consider a SHG image $f_{\mathrm{SHG}}(x,y)$ containing fibers of collagen. This is a gray-scale image where $f_{\mathrm{SHG}}(x,y)=0$ and $f_{\mathrm{SHG}}(x,y)=255$ correspond to black and white pixel levels, respectively, and for which the Euclidean norm can be written as

$$\|f_{\mathrm{SHG}}\| = \sqrt{\langle f_{\mathrm{SHG}}, f_{\mathrm{SHG}}\rangle}. \tag{1}$$

Then, if the collagen fibers are oriented along a preferential direction, the stronger SHG intensity variation will be along the orthogonal direction. The derivative of f_{SHG} along the direction given by the unitary vector $\vec{u}_\alpha = (\cos\alpha, \sin\alpha)$ can be expressed as

$$D_{\vec{u}_\alpha} f_{\mathrm{SHG}}(x,y) = \vec{u}_\alpha^T \nabla f_{\mathrm{SHG}}(x,y), \tag{2}$$

where $\nabla f_{\mathrm{SHG}}(x,y) = (f_x^{\mathrm{SHG}}, f_y^{\mathrm{SHG}})$ is the gradient of f_{SHG}. Then the direction along which the partial derivative is maximized is given by

$$\vec{u}_\alpha = \arg\ \max \|D_{\vec{u}_\alpha} f_{\mathrm{SHG}}(x,y)\|^2, \tag{3}$$

with

$$\|D_{\vec{u}_\alpha} f_{\mathrm{SHG}}(x,y)\|^2 = \langle \vec{u}_\alpha^T \nabla f_{\mathrm{SHG}}, \nabla f_{\mathrm{SHG}} \vec{u}_\alpha^T\rangle = \vec{u}_\alpha^T \vec{S}_{\mathrm{SHG}} \cdot \vec{u}_\alpha, \tag{4}$$

and

$$\vec{S}_{\mathrm{SHG}} = \langle \nabla f_{\mathrm{SHG}}, \nabla f_{\mathrm{SHG}}^T\rangle = \begin{bmatrix} \langle f_x^{\mathrm{SHG}}, f_x^{\mathrm{SHG}}\rangle & \langle f_x^{\mathrm{SHG}}, f_y^{\mathrm{SHG}}\rangle \\ \langle f_x^{\mathrm{SHG}}, f_y^{\mathrm{SHG}}\rangle & \langle f_y^{\mathrm{SHG}}, f_y^{\mathrm{SHG}}\rangle \end{bmatrix}. \tag{5}$$

This 2×2 matrix, $\vec{S}_{\mathrm{SHG}}$, is called the structure tensor. Its elements are the partial derivatives of f_{SHG} along the x and y directions. The directional derivative is maximized along the direction corresponding to the maximum eigenvector of $\vec{S}_{\mathrm{SHG}}$ with an associated eigenvalue $\lambda_{\max} = \max \|D_{\vec{u}_\alpha} f_{\mathrm{SHG}}(x,y)\|^2$. Likewise, the minimum corresponds to the orthogonal direction, and the eigenvalue is given by $\lambda_{\min} = \min \|D_{\vec{u}_\alpha} f_{\mathrm{SHG}}(x,y)\|^2$. As a rule, these eigenvalues verify that $\lambda_{\max} \geq \lambda_{\min} \geq 0$.

Once the structure tensor and its associated eigenvalues are computed, the preferential orientation (PO) can be calculated as [25]

$$\mathrm{PO} = \frac{1}{2}\cdot a\tan\left(\frac{2\langle f_x^{\mathrm{SHG}}, f_y^{\mathrm{SHG}}\rangle}{\langle f_y^{\mathrm{SHG}}, f_y^{\mathrm{SHG}}\rangle - \langle f_x^{\mathrm{SHG}}, f_x^{\mathrm{SHG}}\rangle}\right). \tag{6}$$

In this work, the standard deviation of PO across the SHG image is defined as the structural dispersion (SD) of the collagen fibers. The eigenvalues of the structure tensor have been reported to allow the calculation of the parameters of linear symmetry [32] or image corner detection [33]. Moreover, we propose the contrast of the eigenvalues as a measurement of the amount of linear symmetry of the collagen fiber spatial distribution. This parameter is called degree of isotropy (DoI) and can be written as

$$\mathrm{DoI} = \left(\frac{\lambda_{\max} - \lambda_{\min}}{\lambda_{\max} + \lambda_{\min}}\right)^2. \tag{7}$$

These parameters can be used to characterize the collagen fiber structural organization of an SHG image at a global scale (i.e., using the entire image, usually 210 μm × 210 μm in this work) or at a local scale (an area of 20 μm × 20 μm). In this sense, the ratio of isotropy (RoI) is defined as

$$\mathrm{RoI} = \left(\frac{\mathrm{DoI}_{\mathrm{Local}}}{\mathrm{DoI}_{\mathrm{Global}}}\right). \tag{8}$$

This parameter provides values higher (lower) than 1 when the local structure is more (less) organized than the global one. An isotropic sample presents an RoI = 1.

B. Experimental System: SHG Microscope

Figure 1 shows a schematic diagram of the experimental system used for SHG imaging and described in detail in [34].

Briefly, a mode-locked Ti:sapphire femtosecond laser (λ_ω = 760 nm, 76 MHz, 120-fs pulses) used as an illumination source was coupled into a commercially available microscope. The laser beam reached the sample through a nonimmersion long working distance microscope objective (20× and NA = 0.5). The averaged power of the laser beam depended on the sample (100–170 mW/cm^2). A photomultiplier tube recorded the SHG signal from the (collagen-based) sample, detected in the backward direction, after being transmitted through a dichroic mirror (DM) and a narrowband spectral filter (380 ± 10 nm, SHG filter). SHG images were acquired in the x–y plane by means of a scanning unit composed of a pair of nonresonant galvanometric mirrors. In addition, a z-scan motor was used to move the microscope objective to the location depth of interest

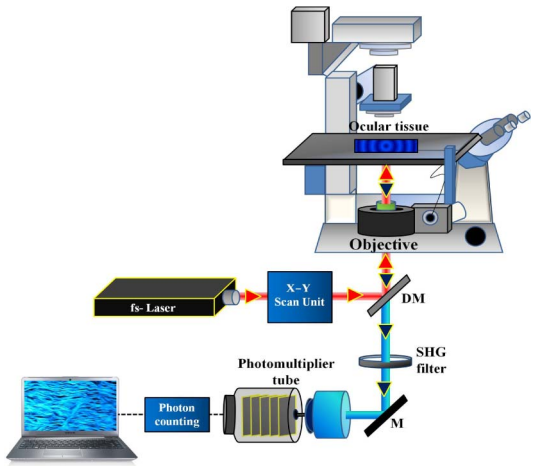

Fig. 1. Schematic diagram of the multiphoton microscope used to record SHG images of collagen-based ocular tissues. M, mirror; DM, dichroic mirror.

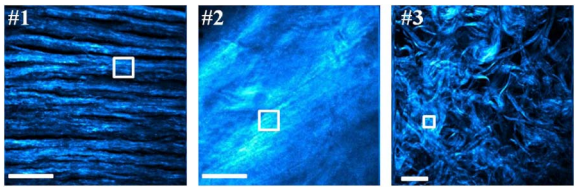

Fig. 2. Experimental SHG images of different collagen-based specimens showing different organizations. The squared areas are the regions of interest that define the local scale (size 20 μm × 20 μm) and were randomly chosen. Bar length: 50 μm.

within the sample. The scanned area was 210 μm × 210 μm (250 × 250 pixels), and the acquisition rate was 1 s per image.

C. Samples and Procedure

SHG images from nonstained ocular tissues composed of type-I collagen were acquired. In particular the specimens corresponded to a 5-μm histological section of human sclera (sample #1), an *ex vivo* human cornea (sample #2), and *ex vivo* bovine sclera (sample #3). As qualitatively shown in Fig. 2, each sample presented collagen fibers with different spatial organizations: lying mainly along the $\hat{x}$ axis (#1), a partially organized distribution (#2), and a nonorganized distribution (#3). To reduce noise, each analyzed SHG image was the average of three individual frames. The image processing was carried out with homemade Matlab software.

3. RESULTS

A. Validation of the Structure Tensor Procedure

In order to test the accuracy of the structure tensor, this was used to analyze artificial images containing elongated structures with different spatial distributions. As a first example, the procedure was applied to a sample composed of vertical lines with different gray levels. From left to right, Fig. 3 shows the original image, the spatially resolved eigenvalues (λ_{max} and λ_{min}), and the DoI map. The structural organization provides an averaged DoI value of 0.96 ± 0.07. The map of PO and the corresponding histogram are depicted at the bottom. As expected from the original image, the mean value of PO was 90° with a small SD, 1°.

The procedure was also tested in another sample providing a more complex arrangement (i.e., partially aligned distribution).

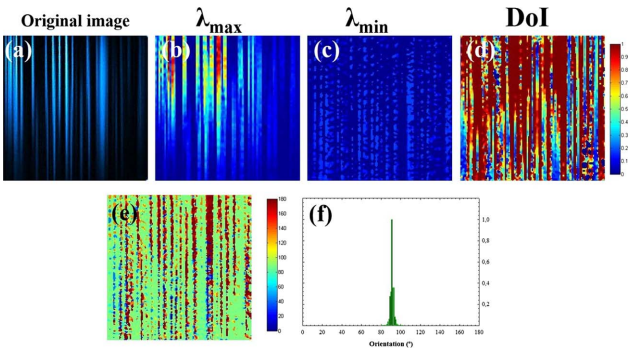

Fig. 3. (a) Original image; (b), (c) spatially resolved eigenvalues; (d), (e) DoI and DO maps; and (f) distribution histogram.

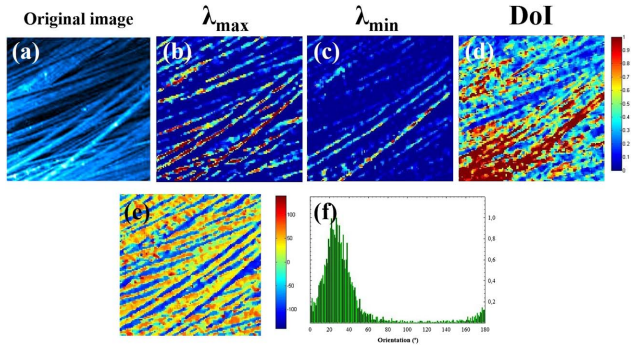

Fig. 4. (a) Original image with partially aligned structures; (b), (c) eigenvalue maps; (d) DoI; (e) map of PO; and (f) distribution histogram.

The original image together with the eigenvalues and the spatially resolved DoI (mean = 0.72 ± 0.20) are shown in Fig. 4. The PO map and the distribution histogram are also included. The average PO across the image was 26° (SD = 13°). Compared to Fig. 3(f), it can be seen how the histogram broadens (i.e., SD increases) due to the fact that the structures are not as well aligned as those of Fig. 3.

B. Classification of Collagen-based Samples According to their Spatial Distribution

1. Collagen Arranged along a Preferential Direction

Figure 5 presents the spatially resolved eigenvalues [Figs. 5(a) and 5(b)] and the DoI map [Fig. 5(c)] corresponding to sample #1. A visual inspection reveals that $\lambda_{max} \gg \lambda_{min}$. This means that a preferential direction exists and is parallel to λ_{max} (λ_{min} would be zero for the ideal case of having fibers perfectly aligned along the horizontal direction). The averaged DoI calculated across the entire image was 0.83 ± 0.15. The map of PO [Fig. 5(d)] clearly displays the fiber organization (mean PO = −5°, SD = 13°). The corresponding PO histogram [Fig. 5(e)] has been fitted by a Gaussian curve with a correlation of $R^2 = 0.97$, where the peak of the curve corresponds to the mean value of PO.

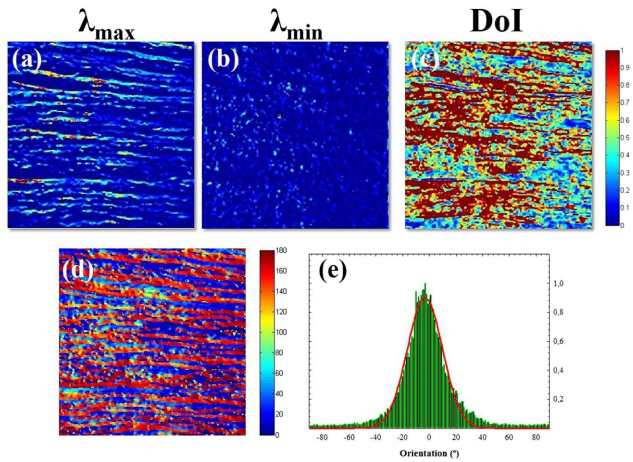

Fig. 5. (a), (b) Eigenvalues; (c) DoI; (d) PO maps; and (e) distribution histogram. The red line in the histogram corresponds to the best Gaussian fit.

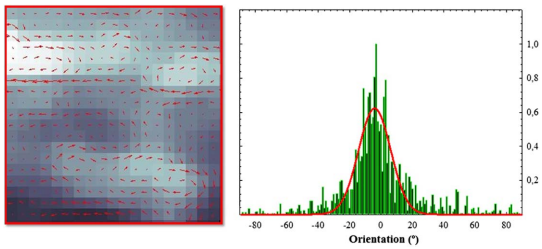

Fig. 6. Map of PO at local scale (sample #1) and corresponding distribution histogram fitted to a Gaussian function.

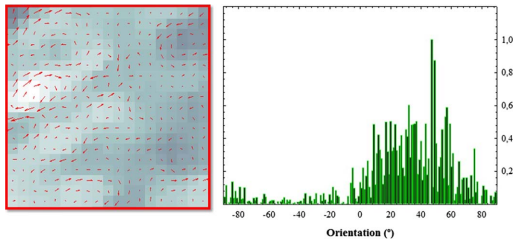

Fig. 8. Map of PO and distribution histogram computed over the region of interest marked in Fig. 2 (sample #2).

To analyze the relationship between global and local scales, the parameters associated with the structure tensor were computed in the squared region of interest marked in sample #1 (see Fig. 2). The averaged DoI across this local region image was 0.79 ± 0.20 (not shown), which indicates the presence of an organized collagen structure. Figure 6 shows the distribution of PO for that local area (mean PO = −9°, SD = 13°). For a better understanding this has been represented by means of vectors overwritten (pixel by pixel) on the selected region of interest. On the right panel the corresponding histogram is depicted together with the best fit to a Gaussian curve ($R^2 = 0.90$). When comparing global and local areas through the RoI, the value found was 0.94. This value is close to 1 and indicates that the organization of collagen is similar for both scales (global and local), that is, the sample presents a homogeneous distribution.

2. Partially Organized Collagen Pattern

For sample #2, Fig. 7 shows the eigenvalues [Figs. 7(a) and 7(b)] and the DoI map [Fig. 7(c)]. The DoI averaged across the entire image was 0.20 ± 0.35, much smaller than the value in Fig. 5. This is associated with a partial loss of order within the collagen fibers, and it is also related to an increase in the values of both λ_{min} and SD. Figures 7(d) and 7(e) depict the map of PO (PO = 33°, SD = 40°) and the distribution histogram, respectively. Similar to sample #1, this histogram also presents a preferential orientation; however, the dispersion is much higher for this sample #2 due to its spatial organization.

When taking into account a local scale (i.e., region of interest of Fig. 2), the structural organization showed an increase ($DoI_{Local} = 0.53 \pm 0.13$) compared to the global scale. Moreover, the collagen orientation of this sample was preserved (mean PO = 34°), and the SD decreases up to 23°. Figure 8 shows the PO map and the corresponding distribution histogram at local scale. This increase in organization from a local to a global scale is clearly shown in the value of the RoI (2.5).

3. Nonaligned Collagen Distribution

As explained above, sample #3 corresponds to a collagen-based tissue where the fibers present a nonorganized distribution. The maps of eigenvalues and DoI are depicted in Fig. 9. In this case, fibers can be organized along any direction, $\lambda_{max} \approx \lambda_{min} \geq 0$. The averaged DoI value at this global scale was 0.09 ± 0.11. The averaged PO value can be computed from Fig. 9(d), but this has no physical meaning, since there is not a preferred orientation of the fibers. This can be seen in the distribution histogram [Fig. 9(e)]. Moreover, the distribution presents a high dispersion (SD = 54°) related to the absence of arrangement along a particular direction.

However, when the structure tensor is applied to a region of interest (see Fig. 2), the averaged DoI_{Local} increased up to 0.53 ± 0.24, indicating that the local scale presents a higher organization than the global one. The corresponding RoI for this sample was RoI = 5.89. The increase in DoI was associated with a decrease in SD (23°) and the presence of a PO (at 45°, as shown in Fig. 10).

C. Relationship between DoI and SD

Since SD was defined as the standard deviation of PO across the entire image (or the region of interest), it can be thought that

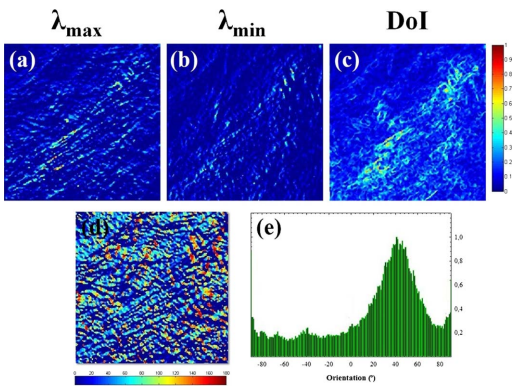

Fig. 7. (a), (b) Maps of eigenvalues; (c), (d) DoI and PO maps, respectively; and (e) distribution histogram for sample #2.

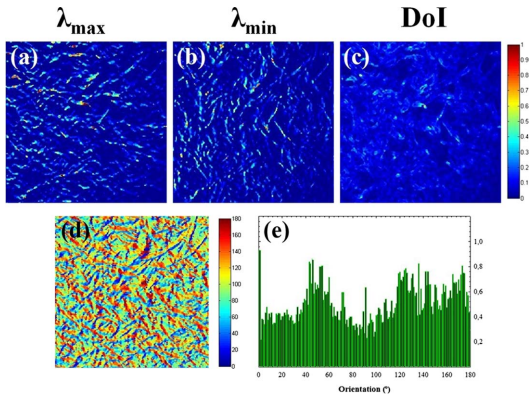

Fig. 9. (a), (b) Eigenvalues; (c), (d) DoI and PO maps, respectively; and (e) distribution histogram for sample #3.

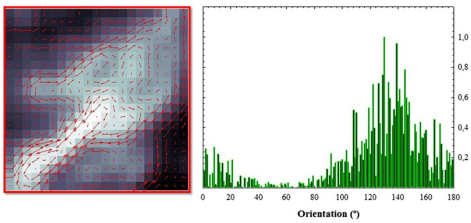

Fig. 10. Map of PO and corresponding distribution histogram at local scale (sample #3).

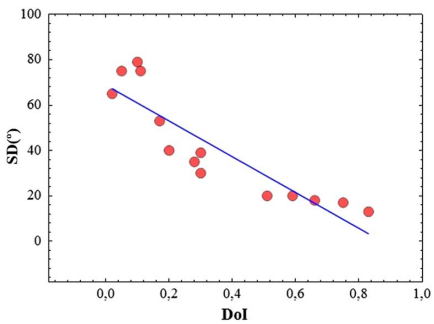

Fig. 11. SD versus DoI for 14 different samples.

the higher the SD, the higher the dispersion of the fibers and the lower the DoI. Then the question would be, is there any relationship between SD and DoI? To answer this question the structure tensor was used to compute both parameters in 14 collagen-based specimens. These samples corresponded to corneas and pieces of sclera of different species, such as rabbit, pig, and chicken, among others (samples #1, #2, and #3 were also included in the set). Figure 11 shows the results, where a significant linear correlation ($R^2 = 0.89$ and $p < 0.0001$) between SD and DoI was found.

4. DISCUSSION AND CONCLUSIONS

We have developed a method based on the structure tensor to compute isotropy parameters such as DoI, PO, and SD in SHG images of collagen-based tissues. Moreover, the RoI parameter has been defined to compare the fiber arrangement at both global and local scales. This parameter might be useful to understand the relationship between the collagen distributions at both scales. This procedure allows the objective classification of collagen distributions. Throughout this work special emphasis was made on ocular tissues.

Results show that when a collagen distribution is parallel arranged, λ_{max} corresponds to the PO and $\lambda_{min} \sim 0$, DoI $\geq$ 0.70 and $0° \leq$ SD $\leq 20°$. The distribution histogram computed from PO maps can be fitted by a Gaussian curve. Moreover, the value of the RoI was close to 1, which means that the organization is similar at both local and global scales.

For partially organized samples, $0.20 \leq$ DoI < 0.70 and $20° <$ SD $\leq 40°$. For this distribution the collagen still preserves a PO corresponding to λ_{max}, although λ_{min} increases (because of the increase of the SD). When reducing the area of analysis, the collagen organization increases (RoI = 2.55) for sample #2. In other words, local structures present lower SD (higher DoI) than the global ones.

Table 1. Objective Classification of Collagen Distribution through the Structure Tensor

Arranged along a PO	Partially Organized	Disorganized
DoI $\geq$ 0.70 $0° \leq$ SD $\leq 20°$	$0.20 \leq$ DoI < 0.70 $20° <$ SD $\leq 40°$	DoI < 0.20 SD $> 40°$

When the external organization decreases significantly, the SD increases and the sample does not present any preferential collagen orientation. For these nonorganized samples, $\lambda_{max} \sim \lambda_{min} \geq 0$, DoI < 0.20, and SD $> 40°$. Moreover, the distribution histograms appear homogeneous due to the absence of a PO. Similarly to partially organized samples, at local scale the organization is higher and a PO can also be found, although with lower SD than that corresponding to well-organized samples. For a better understanding, Table 1 summarizes the results reported here. In this work all samples correspond to ocular tissues and the different types of organization that can be found in them.

Most studies on collagen architecture have been carried out in a qualitative manner. In a particular case such as the cornea, the quantitative method here reported might help to analyze the changes produced in collagen organization due to high levels of intraocular pressure [35], after surgery [36–39], and as a result of external damage [40,41]. This method might also be used in early detection and tracking of pathological processes [42,43].

Although there are several techniques to analyze the collagen spatial distribution, the FFT is one of the most extended. It has been used with SHG images to analyze the corneal collagen organization [40], stromal changes in corneas affected by keratoconus [44], and lamellar spatial distribution in combination with adaptive optics [45].

If a given image shows fibers arranged in a dominant orientation, the spatial frequencies of the FFT spectrum are aligned along the orthogonal direction [46,47]. When using the FFT to analyze SHG images containing collagen structures, the resolution of the FFT is limited by the image noise, and usually image filtering is required. In general, the distributions of the FFT spatial frequencies are fitted to an ellipse, and the ratio between its axes is used as a parameter to calculate changes in collagen organization. The more random a collagen distribution is, the better the fit to a circle.

Compared to the FFT procedure, the method based on the structure tensor reported here has several advantages as an alternative technique for quantification of collagen organization: (1) It is directly applied over the SHG images, pixel by pixel, without the need of postprocessing and image filtering, and (2) the spatially resolved eigenvalues allow discrimination of not only the areas of maximum organization (λ_{max}) but also those where the orientation is not significant.

In conclusion, the procedure based on the structure tensor described here provides a useful tool to characterize and quantify collagen organizations. A special emphasis was put on the analysis of the distributions of collagen fiber in ocular tissues, but the procedure can be applied on any collagen-based tissue.

A linear correlation was found between DoI and SD. This finding objectively demonstrates that the higher the collagen organization, the lower the structural dispersion. The proposed method can be used as a useful tool in clinical diagnosis of pathologies related with collagen disorders.

Funding. European Regional Development Fund (EU-FEDER); Secretaría de Estado de Investigación, Desarrollo e Innovación (SEIDI) (FIS2013-41237-R).

REFERENCES

1. R. Seeley, T. Stephens, and P. Tate, *Anatomy and Physiology* (McGraw-Hill, 2003).
2. H. Lodish, A. Berk, S. L. Zipursky, P. Matsudaira, D. Baltimore, and J. Darnell, *Molecular Cell Biology* (2000).
3. G. A. Holzapfe, T. C. Gasser, and R. W. Ogden, "Comparison of a multilayer structural model for arterial walls with a Fung-type model, and issues of material stability," J. Biomech. Eng. **126**, 264–275 (2004).
4. D. J. Prockop and K. I. Kivirikko, "Collagens: molecular biology, diseases and potentials for therapy," Annu. Rev. Biochem. **64**, 403–434 (1995).
5. A. J. M. Spencer, *Continuum Theory of the Mechanics of Fibre-Reinforced Composites* (Springer, 1984).
6. J. Diamant, A. Keller, E. Baer, M. Litt, and R. G. C. Arridge, "Collagen: ultrastructure and its relation to mechanical properties as a function of ageing," Proc. R. Soc. London Ser. B **180**, 293–315 (1972).
7. M. Comninou and I. V. Yannas, "Dependence of stress–strain nonlinearity of connective tissues on the geometry of collagen fibers," J. Biomech. **9**, 427–433 (1976).
8. Y. Lanir, "Structure–strength relations in mammalian tendon," Biophys. J. **24**, 541–554 (1978).
9. P. J. Campagnola, H. A. Clark, W. A. Mohler, A. Lewis, and L. M. Loew, "Second-harmonic imaging microscopy of living cells," J. Biomed. Opt. **6**, 277–286 (2001).
10. B. F. Hochheimer, "Second harmonic light generation in the rabbit cornea," Appl. Opt. **21**, 1516–1518 (1982).
11. M. Han, G. Giese, and J. Bille, "Second harmonic generation imaging of collagen fibrils in cornea and sclera," Opt. Express **13**, 5791–5797 (2005).
12. S. W. Teng, H. Y. Tan, J. L. Peng, H. H. Lin, K. H. Kim, W. Lo, Y. Sun, W. C. Lin, S. J. Lin, S. H. Jee, P. T. C. So, and C. Y. Dong, "Multiphoton autofluorescence and second-harmonic generation imaging of the *ex vivo* porcine eye," Invest. Ophthalmol. Visual Sci. **47**, 1216–1224 (2006).
13. N. Morishige, W. M. Petroll, T. Nishida, M. C. Kenney, and J. V. Jester, "Noninvasive corneal stromal collagen imaging using two-photon-generated second-harmonic signals," J. Cataract Refractive Surg. **32**, 1784–1791 (2006).
14. J. M. Bueno, E. J. Gualda, and P. Artal, "Analysis of corneal stroma organization with wavefront optimized nonlinear microscopy," Cornea **30**, 692–701 (2011).
15. P. J. Campagnola, "Second harmonic generation imaging microscopy: applications to diseases diagnostics," Anal. Chem. **83**, 3224–3231 (2011).
16. D. Aït-Belkacem, M. Guilbert, M. Roche, J. Duboisset, P. Ferrand, G. Sockalingum, P. Jeannesson, and S. Brasselet, "Microscopic structural study of collagen aging in isolated fibrils using polarized second harmonic generation," J. Biomed. Opt. **17**, 080506 (2012).
17. G. Latour, I. Gusachenko, L. Kowalczuk, I. Lamarre, and M. C. Schanne-Klein, "*In vivo* structural imaging of the cornea by polarization-resolved second harmonic microscopy," Biomed. Opt. Express **3**, 1–15 (2012).
18. J. C. Marini, A. Forlino, W. A. Cabral, A. M. Barnes, J. D. San Antonio, S. Milgrom, J. C. Hyland, J. Korkko, D. J. Prockop, and A. Paepe, "Consortium for osteogenesis imperfecta mutations in the helical domain of type I collagen: regions rich in lethal mutations align with collagen binding sites for integrins and proteoglycans," Hum. Mutat. **28**, 209-221 (2007).
19. M. M. Johns, V. Kolachala, E. Berg, S. Muller, F. X. Creighton, and R. C. Branski, "Radiation fibrosis of the vocal fold: from man to mouse," Laryngoscope **122**, S107–S125 (2012).
20. J. L. Alio, A. Artola, A. Hassanein, H. Haroun, and A. Galal, "One or 2 Intacs segments for the correction of keratoconus," J. Cataract Refractive Surg. **31**(5), 943–953 (2005).
21. H. Schomberg and J. Timmer, "The gridding method for image-reconstruction by Fourier transformation," IEEE Trans. Med. Imag. **14**, 596–607 (1995).
22. H. G. Adelmann, "Butterworth equations for homomorphic filtering of images," Comp. Biol. Med. **28**, 169–181 (1998).
23. Y. Mega, M. Robitaille, R. Zareian, J. McLean, J. Ruberti, and C. DiMarzio, "Quantification of lamellar orientation in corneal collagen using second harmonic generation images," Opt. Lett. **37**, 3312–3314 (2012).
24. J. M. Bueno, R. Palacios, M. K. Chessey, and H. Ginis, "Analysis of spatial lamellar distribution from adaptive-optics second harmonic generation corneal images," Biomed. Opt. Express **4**, 1006–1013 (2013).
25. B. Jahne, *Spatio-Temporal Image Processing: Theory and Scientific Applications* (Springer, 1993).
26. J. Weickert, *Anisotropic Diffusion in Image Processing* (Teubner, 1998).
27. M. Rouson, T. Brox, and R. Deriche, "Active unsupervised texture segmentation on a diffusion based feature space," IEEE Conf. Comput. Vis. Pattern Recogn. **2**, 699–706 (2003).
28. J. Bigun, T. Bigun, and K. Nilsson, "Recognition by symmetry derivatives and the generalized structure tensor," IEEE Trans. Pattern Anal. Mach. Intell. **26**, 1590–1605 (2004).
29. W. Förstner and E. Gulch, "A fast operator for detection and precise location of distinct points, corners and centres of circular features," in *International Society for Photogrammetry and Remote Sensing (ISPRS) Intercommission Conference on Fast Processing of Photogrammetric Data*, Interlaken, 1987, pp. 281–305.
30. A. D. Freed, D. R. Einstein, and I. Vesely, "Invariant formulation for dispersed transverse isotropy in aortic heart valves," Biomech. Model. Mechanobiol. **4**, 100–117 (2005).
31. T. C. Gasser, R. W. Ogden, and G. A. Holzapfel, "Hyperelastic modeling of arterial layers with distributed collagen fibre orientations," J. R. Soc. Interface **3**, 15–35 (2006).
32. J. Bigün, "Pattern recognition in images by symmetries and coordinate transformations," Comput. Vis. Image Underst. **68**, 290–307 (1997).
33. C. Harris and M. Stephens, "A combined corner and edge detector," in *Proceedings of Fourth Alvey Vision Conference* (1988), pp. 23.1–23.6.
34. J. M. Bueno, E. J. Gualda, and P. Artal, "Adaptive optics multiphoton microscopy to study ex vivo ocular tissues," J. Biomed. Opt. **15**, 066004 (2010).
35. Q. F. Wu and A. T. Yeh, "Rabbit cornea microstructure response to changes intraocular pressure visualized by using nonlinear optical microscopy," Cornea **27**, 202–208 (2008).
36. K. Plamann, F. Aptel, C. L. Arnold, A. Courjaud, C. Crotti, F. Deloison, F. Druon, P. Georges, M. Hanna, J. M. Legeais, F. Morin, É. Mottay, V. Nuzzo, D. A. Peyrot, and M. Savoldelli, "Ultrashort pulse laser surgery of the cornea and the sclera," J. Opt. **12**, 084002 (2010).
37. E. J. Gualda, J. R. Vázquez de Aldana, M. C. Martínez-García, P. Moreno, J. Hernández-Toro, L. Roso, P. Artal, and J. M. Bueno, "Femtosecond infrared intrastromal ablation and backscattering-mode adaptive-optics multiphoton microscopy in chicken corneas," Biomed. Opt. Express **2**, 2950–2960 (2011).
38. P. Steven, M. Hovakimyan, R. F. Guthoff, G. Hüttmann, and O. Stachs, "Imaging corneal crosslinking by autofluorescence 2-photon microscopy, second harmonic generation, and fluorescence lifetime measurements," J. Cataract Refractive Surg. **36**, 2150–2159 (2010).
39. J. M. Bueno, A. Giakoumaki, E. J. Gualda, F. Schaeffel, and P. Artal, "Analysis of the chicken retina with an adaptive optics multiphoton microscope," Biomed. Opt. Express **2**, 1637–1648 (2011).
40. P. Matteini, F. Ratto, F. Rossi, R. Cicchi, C. Stringari, D. Kapsokalyvas, F. S. Pavone, and R. Pini, "Photothermally-induced

disordered patterns of corneal collagen revealed by SHG imaging," Opt. Express **17**, 4868–4878 (2009).
41. W. Lo, Y. L. Chang, J. S. Liu, C. M. Hseuh, V. Hovhannisyan, S. J. Chen, H. Y. Tan, and C. Y. Dong, "Multimodal, multiphoton microscopy and image correlation analysis for characterizing corneal thermal damage," J. Biomed. Opt. **14**, 054003 (2009).
42. N. Morishige, A. J. Wahlert, M. C. Kenney, D. J. Brown, K. Kawamoto, T. Chikama, T. Nishida, and J. V. Jester, "Second-harmonic imaging microscopy of normal human and keratoconus cornea," Invest. Ophthalmol. Visual Sci. **48**, 1087–1094 (2007).
43. S. J. Lin, C. H. Hsiao, Y. F. Chen, S. C. M. Huang, W. C. Lin, S. H. Jee, H. S. Yu, and C. Y. Dong, "Multiphoton fluorescence and second harmonic generation imaging of the structural alterations in keratoconus ex vivo," Invest. Ophthalmol. Visual Sci. **47**, 5251–5259 (2006).
44. W. Lo, W. L. Chen, C. M. Hsueh, A. A. Ghazaryan, S. J. Chen, D. H. K. Ma, C. Y. Dong, and H. Y. Tan, "Fast Fourier transform–based analysis of second-harmonic generation image in keratoconic cornea," Invest. Ophthalmol. Visual Sci. **53**, 3501–3507 (2012).
45. J. M. Bueno, R. Palacios, M. K. Chessey, and H. Ginis, "Analysis of spatial lamellar distribution from adaptive-optics second harmonic generation corneal images," Biomed. Opt. Express **4**, 1006–1013 (2013).
46. J. W. Goodman, *Introduction to Fourier Optics* (McGraw-Hill, 1996).
47. J. C. Russ, *The Image Processing Handbook* (CRC Press, 2007).